Computational Materials Science 244 (2024) 113176

Contents lists available at ScienceDirect

Computational Materials Science

journal homepage: www.elsevier.com/locate/commatsci

Full Length Article

High pressure and high temperature behaviour of alkali-halide fluorite CaF_2 for technological applications

Gianfranco Ulian, Giovanni Valdrè *

Dipartimento di Scienze Biologiche, Geologiche e Ambientali, Università di Bologna, Piazza Porta San Donato 1, I-40126, Bologna, Italy

ARTICLE INFO

Keywords:
Fluorite
cubic CaF_2
Thermodynamics
Elastic properties
Density Functional Theory
Quasi-harmonic approximation

ABSTRACT

Fluorite (CaF_2, space group $Fm\bar{3}m$) is an alkali-earth halide mineral with important and manyfold technological applications and for these means several experimental and theoretical investigations were performed to characterize the structural, electronic, optical, and elastic properties. However, a detailed knowledge of the thermodynamics and thermoelastic properties of fluorite in a wide temperature and pressure range is still missing. In this work, density functional theory simulations using the hybrid B3LYP functional and all-electron Gaussian-type orbitals basis sets were employed to model these properties between 0 – 1000 K and from 0 GPa to 7 GPa. The calculated *PVT* equation of state parameters were $V_{0T} = 42.278(7)$ Å^3, $K_{0T} = 92.14(7)$ GPa, $K'_{0T} = 3.56(2)$ using a 3rd-order Birch-Murnaghan formulation, $\alpha_0 = 7.84(2) \times 10^{-5}$ K^{-1} and $\alpha_1 = 2.17(3) \times 10^{-5}$ K$^{-1/2}$ from a modified Holland and Powell thermal equation of state, and a variation of the bulk modulus with temperature $\partial K_{0T}/\partial T = -0.0160(1)$ GPa K^{-1}. The quality of the theoretical results was assessed by comparison with the few available data reported in the scientific literature, finding a general good agreement and extending the knowledge on this important technological material.

1. Introduction

Fluorite (CaF_2, Fig. 1) is one of the simple alkali halide minerals that at room conditions belongs to the cubic crystal system (space group *Fm-3 m*). From the mineralogical, crystal-chemical and solid-state physics perspectives, fluorite represents a prototype phase because of both its pure ionic nature and its crystal structure that is shared with other metal halides (e.g., SrF_2 and BaF_2), sulphides, oxides, metallic alloys and other intermetallic compounds [1]. Fluorite and other alkaline-earth fluorides present a very large band gap ($E_g > 10$ eV), hence they are transparent in a wide range of radiation wavelength, explaining their application, to cite an example, as window materials for both infrared and ultraviolet wavelengths. Calcium fluoride is also employed in the production of lenses and optical fibres because of its optical isotropy, chemical stability and elastic properties [2–4].

Other application of fluorite in Earth and materials science is its use as a pressure standard for the calibration of high-pressure and high-temperature X-ray diffraction (XRD) measurements [5–7]. For these experiments, it is of utmost importance knowing the equation of state of fluorite, i.e., the function that correlates the pressure with the unit cell volume of the mineral, which in turn is used to accurately determine the pressure state inside the diamond-anvil cell [8]. This halide mineral allows the high-pressure XRD experiments up to moderate pressures because it was shown that the cubic structure of CaF_2 changes to the $PbCl_2$-type one belonging to the *Pbnm* space group (orthorhombic) at 9.5 GPa, a phase that is stable up to 45 GPa at room temperature [9].

Cubic CaF_2 was also subject of several quantum mechanical studies at different levels of theory and approximations, i.e., tight-binding with orthogonalized plane-waves [10], Hartree-Fock (HF) with linear combination of atomic orbitals (LCAO) basis sets [11], density functional theory (DFT) with several functionals and both LCAO and plane waves basis sets [12–15], to obtain the structural, elastic, electronic and optical properties, and how atomic substitutions (e.g., the formation of H centres) may affect them. In this context, fluorite is a suitable testing phase to investigate the accuracy and limitations of different theoretical approaches in analysing the properties of pure ionic solid materials.

However, to the authors knowledge, there has not been any theoretical investigation that characterized how the thermodynamics and elastic properties of fluorite are affected by simultaneous variations of pressure and temperature. In addition, attempts to study the behaviour of the mineral at the experimental level using *PVT* equation of state formulations resulted in scattered results because of the different

* Corresponding author.
E-mail address: giovanni.valdre@unibo.it (G. Valdrè).

https://doi.org/10.1016/j.commatsci.2024.113176
Received 10 May 2024; Received in revised form 11 June 2024; Accepted 12 June 2024
Available online 28 June 2024

accuracy of the methods used to obtain the *PV* equation of state, the thermal expansion coefficient, and the isobaric heat capacity. For instance, Hazen and Fingers [5] overestimated the high temperature behaviour because they used the thermal expansion coefficient of Sharma [16], which was anomalously high.

Given the technological importance of this mineral, the present work tries to fill this knowledge gap, presenting a detailed analysis of the thermodynamic and thermoelastic properties between 0 GPa and 7 GPa and in the temperature range 0–1000 K. To this aim, a theoretical approach based on static density functional theory simulations using the quasi-harmonic approximation [17] to include the thermal effects was used. All the relevant quantities necessary to model the thermodynamics of cubic CaF_2, e.g., the evolution of the crystal structure and lattice dynamics with pressure, are reported and discussed against the available data in the scientific literature.

2. Computational methods

2.1. Hamiltonian and computational parameters

The simulations reported in the present work were carried out using the CRYSTAL17 code [18] that implements the Kohn-Sham Density Functional Theory (DFT) framework. The hybrid B3LYP functional [19–21], which includes 20 % of exact Hartree-Fock exchange energy and some non-local contribution to the correlation energy, was used throughout the present study. This functional is very accurate for analysis of the crystal structure, elastic properties and the lattice dynamics of minerals and crystalline materials [22–28], all topics of the present investigation on fluorite. The crystalline orbitals were constructed as linear combination of atomic orbitals, the latter being Gaussian-type orbitals. Calcium and fluorine were described using double-ζ valence basis sets that include polarization functions, specifically developed by Vilela Oliveira and collaborators [29] for solid systems.

The electronic density was integrated on a pruned grid with 75 radial and 974 angular points (XLGRID keyword in CRYSTAL) given by the Gauss-Legendre radial quadrature and Lebedev two-dimensional angular point distribution [30]. An 8 × 8 × 8 Monkhorst-Pack [31] grid of 29 **k** points in the first Brillouin zone (reciprocal space, SHRINK keyword) was used to obtain the total energy with a self-consistent field approach. The tolerance that controls the accuracy of the total energy calculation (TOLDEE) was set to 10^{-8} Ha, whereas the convergence criteria for the evaluation of the Coulomb and pseudo-overlap integrals (TOLINTEG) are controlled by five thresholds called ITOL1–4 and ITOL5 that were set to 10^{-8} and 10^{-16}, respectively. The geometry optimization of the lattice and the internal coordinates was conducted within the same run using the analytical gradient method for the atomic positions and a numerical gradient for the unit cell parameters. The process was considered converged when the gradient and the maximum atomic displacement were lower than 1×10^{-5} Ha bohr^{-1} and 4×10^{-5} bohr, respectively, with respect to the previous optimization step. The convergence criteria were employed successfully in previous works [11,12].

2.2. Vibrational properties

In periodic systems and within the harmonic approximation, the Γ-point (**k** = 0) phonon frequencies are calculated from the mass-weighted Hessian matrix:

$$W_{ij}(\mathbf{k}=0) = \sum_G \frac{H_{ij}^{0G}}{\sqrt{M_i M_j}} \tag{1}$$

where H_{ij}^{0G} is the second derivative of the electronic and nuclear repulsion energy E evaluated at equilibrium $u = 0$ with respect to the displacement of atom A in cell 0 ($u_i = x_i - x_i^*$) and displacement of atom B in cell G ($u_j = x_j - x_j^*$) from their equilibrium position x_i^*, x_j^*:

$$\sum_G H_{ij}^{0G} = \sum_G \left[\frac{\partial^2 E}{\partial u_i^0 \partial u_j^G}\right]_0 \quad i,j = 1,\ldots,3N \tag{2}$$

In CRYSTAL17, the calculation of the Hessian at equilibrium is made by the analytical evaluation of the energy first derivatives, Φ_j, of E with respect to the atomic displacements:

$$\Phi_j = \sum_G \omega_j^G = \sum_G \frac{\partial E}{\partial u_j^G} \quad j = 1,\ldots,3N \tag{3}$$

while second derivatives at $u = 0$ (where all first derivatives are zero) are calculated numerically using a "two-point" formula:

$$\left[\frac{\partial \Phi_j}{\partial u_i^0}\right]_0 \approx \frac{\Phi_j(0,\ldots,u_i^0,\ldots,0) - \Phi_j(0,\ldots,u_i^0,\ldots,0)}{u_i^0} \quad i,j = 1,\ldots,3N \tag{4}$$

The interested reader may find more details on the calculation of the phonon frequencies with CRYSTAL in dedicated literature [32,33].

However, the number of atoms in the primitive cell of fluorite is too small ($N = 3$) for a reliable estimation of the thermodynamic properties of the mineral, as also explained in previous works [22,34,35]. Thus, it is necessary to calculate the phonon dispersion relations by sampling other **k**-points in the first Brillouin Zone other than the central one (**k** = 0), an operation that involved the adoption of a direct-space approach on sufficiently large supercells to converge the harmonic thermodynamic properties [36–38]. In this work, it was checked the effect of increasing supercell sizes, obtained by applying a transformation $\mathbf{M_1}$ or $\mathbf{M_2}$ on the

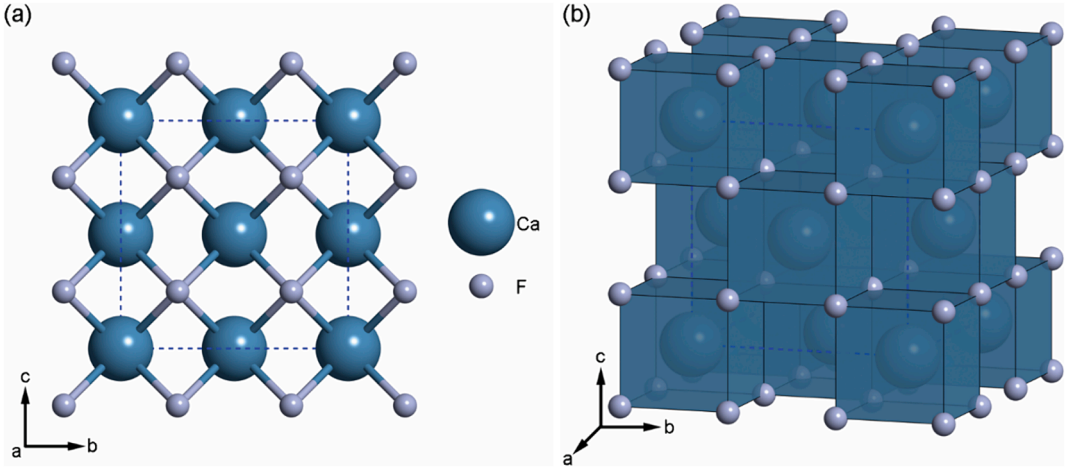

Fig. 1. (a) Ball-and-stick and (b) polyhedral representations of the crystal structure of fluorite CaF_2 (s.g. *Fm-3 m*).

CaF_2 unit cell, as reported in the following:

$$\mathbf{M_1} = \begin{pmatrix} m & 0 & 0 \\ 0 & m & 0 \\ 0 & 0 & m \end{pmatrix} \quad (5)$$

$$\mathbf{M_2} = \begin{pmatrix} -m & m & m \\ m & -m & m \\ m & m & -m \end{pmatrix} \quad (6)$$

The matrix operator of $\mathbf{M_1}$ in Eq. (5) means that the primitive cell is extended $m \times m \times m$ times along the axes which leads to m^3 times N atoms in the supercell. Conversely, $\mathbf{M_2}$ in Eq.(6) involves a primitive →crystallographic cell transformation (3 atoms →12 atoms, see Fig. 1), followed by a $m \times m \times m$ supercell expansion, with $4Nm^3$ atoms in the final cell. It was found that a supercell obtained from $\mathbf{M_1}$ with $m = 3$ (81 atoms in the supercell, 27 **k** points sampled) is large enough to obtain well-converged thermodynamic data (*vide infra*) at affordable computational costs.

Also, given the ionic nature of calcium fluoride, the effect of the longitudinal optical (LO) and transverse optical (TO) splitting in the phonon dispersion was included according to the formulation of Wang et al. [39]. The LO-TO splitting is an effect of long-range Coulomb fields arising from the coherent displacement of the atom nuclei, which is neglected because of the imposed periodic boundary conditions. The calculation of this non-analytical contribution depends on the dielectric tensor ϵ_0 and on the Born effective charge tensor associated with each atom. These quantities were analytically calculated via a coupled-perturbed Kohn-Sham (CPKS) approach [40,41].

2.3. Thermodynamic properties

In the present work, the thermodynamic and thermoelastic properties of cubic fluorite were obtained from the quasi-harmonic approximation (QHA), as well-described in specific literature [17,42,43]. It is known that the lattice dynamics of a crystalline material calculated within the harmonic approximation (HA) leads to vibrational frequencies and thermodynamic quantities that are independent of volume (pressure). This severe approximation provides a wrong description of several physical properties, e.g., the thermal expansion of a unit cell would be zero in the HA framework.

In *ab initio* simulations, the quasi-harmonic approximation (QHA) is a simple, but powerful, method to include the cited dependence of the phonon frequencies on volume. It is not within the scope of the present work to report all the formulations involved in QHA, the interested reader is addressed to dedicated literature [17,22,34]. The calculation of the thermodynamic properties of fluorite within the quasi-harmonic approximation framework was performed using the QUANTAS code [44], which implements the above-mentioned formulations.

3. Results and discussion

3.1. Static equation of state at $T = 0$ K

The compressional behaviour of cubic CaF_2 was investigated using eleven primitive cell volumes between 85 % and 112 % of the equilibrium volume V_0 of fluorite (within the selected computational setting). The energy was calculated at each volume, and the effect of hydrostatic pressure was modelled with a volume-integrated 3rd-order Birch-Murnaghan (BM3) equation of state (EoS) using the $E(V)$ curves as explained by Hebbache and Zemzemi [45,46]:

$$E = E_0 + \frac{9}{16}K_{00}V_{00}\left\{K'_{00}(\eta^2-1)^3 + \left[(\eta^2-1)^2(6-4\eta^2)\right]\right\} \quad \eta = \left(\frac{V_{00}}{V}\right)^{1/3} \quad (7)$$

where η is called dilaton (dimensionless), K_{00} is the bulk modulus, V_{00} the volume at zero pressure and K'_{00} is the pressure first derivative of the bulk modulus. The parameters were obtained at absolute zero (0 K) and no applied pressure (0 GPa), which are indicated in the subscripts used in in Eq. (7). E_0 is the static energy of the unit cell at zero pressure, and, in this case, the second subscript is omitted because in static DFT approach the energy is obtained always at absolute zero Kelvin.

The unit cell structure, the electronic energy E and elastic data are reported in Table 1. The equation of state parameters obtained in athermal conditions were $E_0 = -877.20985(2)$ Ha, $V_{00} = 41.523(14)$ Å^3, $K_{00} = 96.7(5)$ GPa and $K'_{00} = 4.0(1)$. The results suggest that even a second-order BM formulation is sufficient to describe the compressional behaviour of fluorite.

The athermal (zero Kelvin) bulk modulus K_{00} obtained at *ab initio* DFT/B3LYP level of theory is in line with previous simulations carried out using different methods, ranging between 79.5 GPa and 103 GPa [12,47–50].

The obtained BM3 parameters from Eq. (7) were then used to calculate the pressure state at each simulated unit cell volume by using the *PV* formulation of the BM3 equation of state (*vide infra*).

3.2. Electronic properties

The electronic band structure of fluorite CaF_2 is reported in Fig. 2**a**, which was calculated along the Γ – X – U|K – Γ – L – W – X path in the first Brillouin zone (IBZ). According to the simulation results, fluorite is a dielectric material with a large indirect (*X*–Γ) band gap of about 10.52 eV at zero pressure between the *X* and Γ points (see Table 1). The atom-projected density of states shows that the occupied bands are almost entirely pure atomic-like states, with the topmost ones due to the *p* orbitals of the fluoride ion (red line in Fig. 2**a**). Conversely, the conduction bands show a mixing between both Ca and F states, with the major component given by Ca *d* orbitals. In addition, it was shown that the band gap increases almost linearly with pressure, as shown in Fig. 2**b** where the $E_g(P)$ data are graphically reported.

The DFT/B3LYP results are in good agreement with previous data reported in the scientific literature. Using both ultraviolet and X-ray photoelectron spectrometers, Poole and collaborators [51] obtained a separation between the F^- (valence) levels and the Ca^{2+} (conduction) ones of about 17.3(2) eV, whereas a figure of about 10 eV was reported by Harrison [52].

One of the first theoretical study of CaF_2 was performed by Albert and co-workers [10], who employed a combined tight-binding (TB), orthogonalized plane-wave approach to accurately determine the bands structure. Within this semi-empirical approach, the authors obtained a band gap between 16 eV and 12.1 eV depending on the value of the exchange parameter in the TB model. More recently, Kanchana et al. [48] adopted a tight-binding linear muffin tin orbitals approach (TB-LMTO) together within the local density approximation (LDA) to study

Table 1
Fluorite CaF_2 unit cell volume V, lattice parameter a (pc = primitive cell, cc = crystallographic cell), electronic energy E_0 and electronic band gap E_g at different pressures, as obtained from DFT/B3LYP simulations in static conditions.

P (GPa)	a_{cc} (Å)	V_{cc} (Å^3)	V_{pc} (Å^3)	E (Ha)	E_g (eV)
22.1	5.2074	141.206	35.3016	−877.19631	11.55
15.6	5.2736	146.667	36.6668	−877.20211	11.30
10.1	5.3399	152.267	38.0668	−877.20617	11.06
5.3	5.4062	158.008	39.5020	−877.20866	10.83
1.3	5.4725	163.891	40.9729	−877.20976	10.60
0.0	5.4972	166.125	41.5313	−877.20985	10.52
−2.1	5.5388	169.919	42.4798	−877.20962	10.35
−5.0	5.6051	176.093	44.0231	−877.20839	10.13
−7.1	5.6574	181.076	45.2691	−877.20654	9.98
−8.8	5.7089	186.060	46.5150	−877.20437	9.82

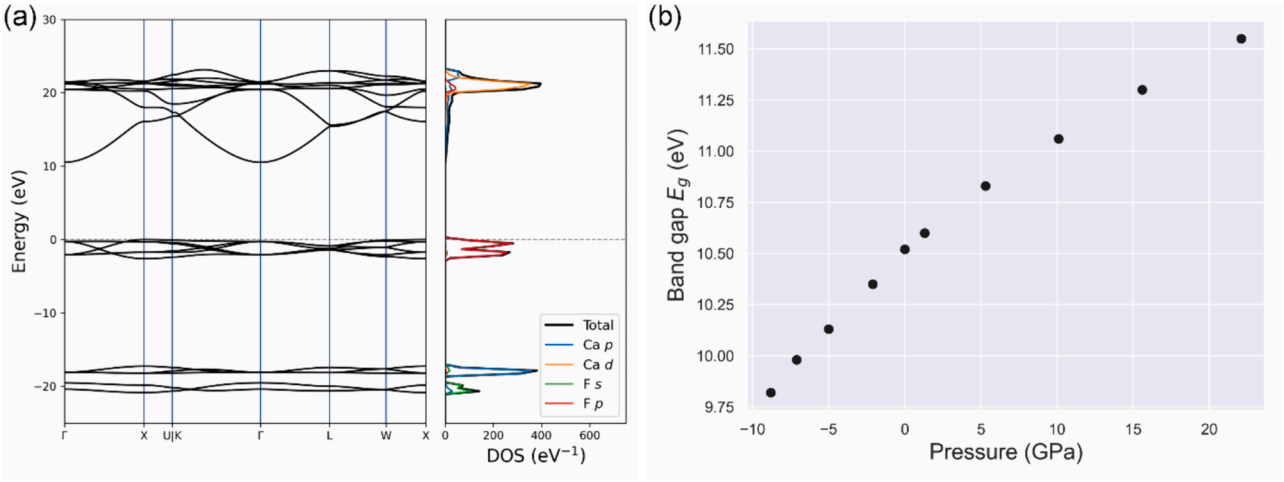

Fig. 2. (a) Electronic band structure (left) and atom-projected density of states (right) of cubic CaF_2 at ambient pressure, as obtained from DFT/B3LYP simulations. (b) Evolution of the calculated electronic band gap energy E_g as a function of pressure.

the electronic properties of cubic CaF_2, obtaining an underestimated band gap of 7.24 eV because of the adopted DFT functional. Similar figures were obtained by Khenata and collaborators [47] using full potential linearized augmented-plane-wave approach (FPLAPW).

Born charges evaluated at Γ-point for the equilibrium geometry of CaF_2 are in agreement with the expected values for an ionic mineral, with $q = +2.090|e|$ and $q = -1.045|e|$ for calcium and fluorine, respectively. The charges showed a very small variation by increasing pressure, with values of $q_{Ca} = +2.110|e|$ and $q_F = -1.055|e|$ at 22.1 GPa, whereas no significant changes were observed by expanding the cell. The atomic charges computed using the DFT/B3LYP approach are in good agreement with the Mulliken population analysis performed by Catti and collaborators [11] at the Hartree-Fock LCAO level of theory. An inspection of the charge density difference (Fig. 3**a**) and total charge density (Fig. 3**b**), computed on the (1 1 0) crystallographic plane, revealed that the electron clouds around the atoms are contracted with respect to those of the free ions. As also suggested by Catti et al. [11], this contraction is due to both the crystal field that compresses the electron clouds and the Pauli's exclusion principle that increases the electron exchange repulsion.

3.3. Phonon properties

The Γ-point ($\mathbf{k} = 0$) phonon modes of fluorite comprise 9 atomic vibrations, which can be subdivided in the following irreducible representations (IRREPs):

$$\Gamma_{tot} = 2F_{1u} + F_{2g} \quad (8)$$

where F modes are triply degenerate and the first F_{1u} mode is associated with acoustic vibrations. Phonons with the "u" subscript (ungerade) are antisymmetric with respect to the inversion centre and are infrared (IR) active, whereas the "g" (gerade) modes are symmetric and active in Raman spectroscopy. The results calculated at the DFT/B3LYP level of theory at different pressures and 0 K are reported in Table 2.

The Raman mode obtained at equilibrium geometry in the present simulation (339.1 cm^{-1}) is in good agreement with the experimental values obtained by Denham et al. [53] and Kassier and co-workers [54], i.e., 328 cm^{-1} and 323 cm^{-1}, respectively. Similarly, the IR-active mode at 288.8 cm^{-1} is in line with the spectroscopic measurement of Lowndess [55] carried out at 5 K (270 cm^{-1}). The slight overestimation of the results (ca. +10 cm^{-1}) is due to the harmonic description of the vibrational motion, which increases the force constants associated with the

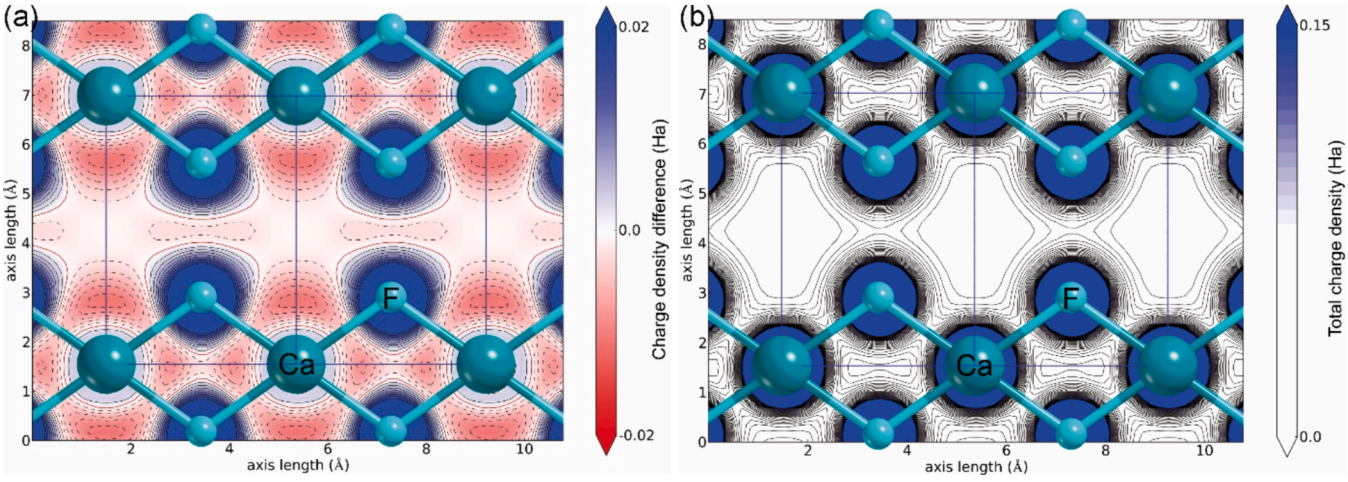

Fig. 3. Maps of the (a) charge density difference and (b) total charge density in fluorite, as observed on the (1 1 0) crystallographic plane. Continuous and dashed black isolines represent positive and negative charge density, respectively, separated by 0.002*e* Ha, whereas the red continuous one shows the zero-charge contour line. The blue lines represent the crystal lattice. (For interpretation of the references to colour in this figure legend, the reader is referred to the web version of this article.)

Table 2
Fluorite vibrational frequencies (in cm^{-1}) as a function of pressure and the mode-Grüneisen parameter (γ_i) obtained from DFT/B3LYP simulations. Experimental (Exp) values at room pressure are reported for a direct comparison.

IRREP	ν (cm^{-1})										γ_i	Exp
P (GPa)	*22.1*	*15.6*	*10.1*	*5.3*	*1.3*	*0.0*	*−2.1*	*−5.0*	*−7.1*	*−8.8*		
F_{1u}	403.7	376.9	352.0	326.3	299.2	288.8	272.1	248.6	233.2	219.7	2.26	270[a]
F_{2g}	429.7	408.1	387.2	367.1	346.9	339.1	326.8	309.4	297.8	286.9	1.49	328[b]

[a] Lowndess [55], results at 5 K;
[b] Denham and collaborators [53], results at 100 K.

different vibrational modes. In previous simulations performed with the B3LYP functional and LCAO basis sets, Mérawa and collaborators [12] obtained 236 cm^{-1} (F_{1u}) and 320 cm^{-1} (F_{2g}), which are slightly lower than those obtained in the present work. It can be suggested that this deviation is due to the different basis set employed by the cited authors (86–511 and 7–311 GTO basis sets for Ca and F, respectively [12]), whereas the one here adopted presents more Gaussian-type functions, which means it is more accurate.

To describe the evolution of phonon modes with volume (pressure), the mode-Grüneisen (or mode-gamma) formulation was employed, whose parameters γ_i are calculated for each i^{th} mode as [17]:

$$\gamma_p = -\frac{\partial \ln \nu_p}{\partial \ln V} = -\frac{V}{\nu_p}\frac{\partial \nu_p}{\partial V} \quad (9)$$

The resulting mode-gamma parameters are reported in Table 2. The only experimentally available mode-gamma result is related to the F_{2g} Raman mode, where $\gamma_i = 1.8$, in agreement with the 1.49 figure obtained from the present theoretical simulations [54,56].

The phonon band structure of CaF_2 at equilibrium geometry calculated along the Γ – X – U|K – Γ – L – W – X path in the IBZ is shown in Fig. 4, which is in line with previous theoretical and experimental investigations [57,58]. This is an important assessment since thermodynamic properties are calculated through statistical mechanics using these dispersion curves.

3.4. Thermodynamic and thermomechanic properties

As explained in detail in the Computational Methods section, the static equation of state results and the calculated phonon dispersion relations at different unit cell volume (pressure) were used to calculate the thermodynamic properties of fluorite by means of the quasi-harmonic approximation. Before the QHA analysis, the numerical convergence of the harmonic properties (entropy S, isochoric heat capacity C_V, internal energy U and Helmholtz free energy F) was carefully checked on different supercell models containing from 3 (number of **k** points equal to 1) to 324 (**k** = 108) atoms. Fig. 5 graphically reports this analysis, showing that the convergence on harmonic thermodynamic data is satisfied with a supercell containing 81 atoms (**k** = 27).

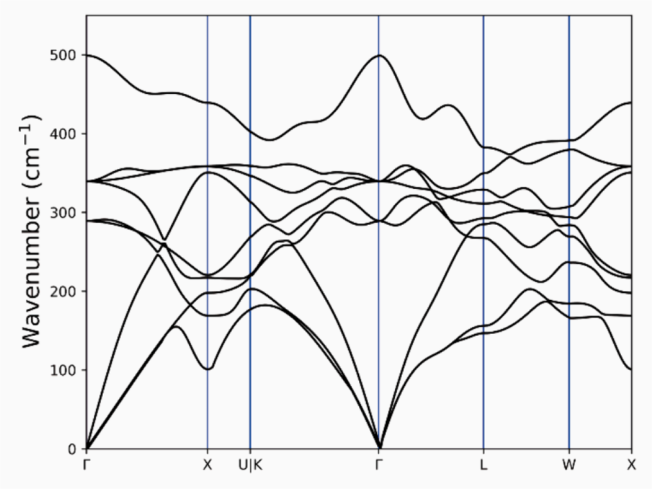

Fig. 4. Phonon band structure of cubic CaF_2 as obtained from DFT/B3LYP simulations.

Within the QHA framework, the evolution of the phonon frequency with volume (pressure) was modelled using a 3rd-order polynomial function for each phonon band of the mineral. The fitting procedure was accurate, with a mean R^2 of 9.997×10^{-1}. Since it is known that cubic CaF_2 undergoes a phase transition at about 9 GPa [6,54,56], the thermodynamic and elastic properties were calculated in a *PT* range of 0–7 GPa and 0–1000 K. Relevant structural, elastic and thermodynamic data at zero pressure and in the range 300–1000 K are reported in Table 3. It is important to remember that the QHA data at 0 K (see Figs. 6-8) are necessarily not the same as in static calculations (*vide supra*) because the zero-point thermal contribution is included in the treatment.

Unit cell volume V_{PT} and the coefficient of volumetric thermal expansion α_V are shown in Fig. 6 as both contour maps and as isobars in the 0 – 1000 K temperature range. No negative thermal expansion was found at low temperatures, and all the curves show the expected trends for the reported quantity. The unit cell volume obtained from the present simulations at 300 K were in line with the experimental measurements of Speziale and Duffy [56], with a general small overestimation of V_{PT} of about 4 %. At the same time, the α_V calculated with density functional theory at $T = 300$ K and $P = 0$ GPa (4.615×10^{-5} K^{-1}) was underestimated by about 20 % with respect to the experimental data (5.7×10^{-5} K^{-1}) of Schumann and Neumann [59].

The bulk modulus K_{PT} of cubic CaF_2 is reported in Fig. 7. The calculated K_{0T} value at 300 K is equal to 91.7 GPa, which is slightly larger than that obtained by experimental high-pressure X-ray diffraction measurements of Angel [6], who specifically calculated $K_{0T} = 81.0$ (1.2) GPa from a Murnaghan equation of state fit. The same consideration can be extended to the more recent measurements of Speziale and Duffy [56], for which a value of 82.0(7) was obtained. As also explained in previous studies [60], this small overestimation is associated to the Hellman-Feynman theorem and the use of LCAO basis sets, which employ atom-centred (localized) Gaussian-type orbitals, i.e., they depend on the nuclei position. It is well-known that when dealing with elastic properties, this approach is affected by the Pulay forces, i.e., the derivative of the basis set with respect to the atomic position, which represents an additional term that should be calculated to obtain more accurate data. However, at the moment, the CRYSTAL code does not allow to evaluate the Pulay forces, which would increase the accuracy of the results.

As can be noted in Fig. 7, the isothermal bulk modulus decreases almost linearly above 300 K, with a slope $\partial K_{0T}/\partial T = -0.0185$ GPa K^{-1} at zero pressure obtained from a 2nd-order polynomial fit of the $K_{0T}(T)$ curves.

Considering a more phenomenological approach, the data calculated from DFT/B3LYP simulations between the temperature and pressure ranges 300–900 K and 0–7 GPa, respectively, were also fitted using the EoSFit7 software [61] to obtain the whole *PVT* equation of state of cubic fluorite. The hydrostatic compression was modelled with the standard BM3 formulation [45], reported in the following

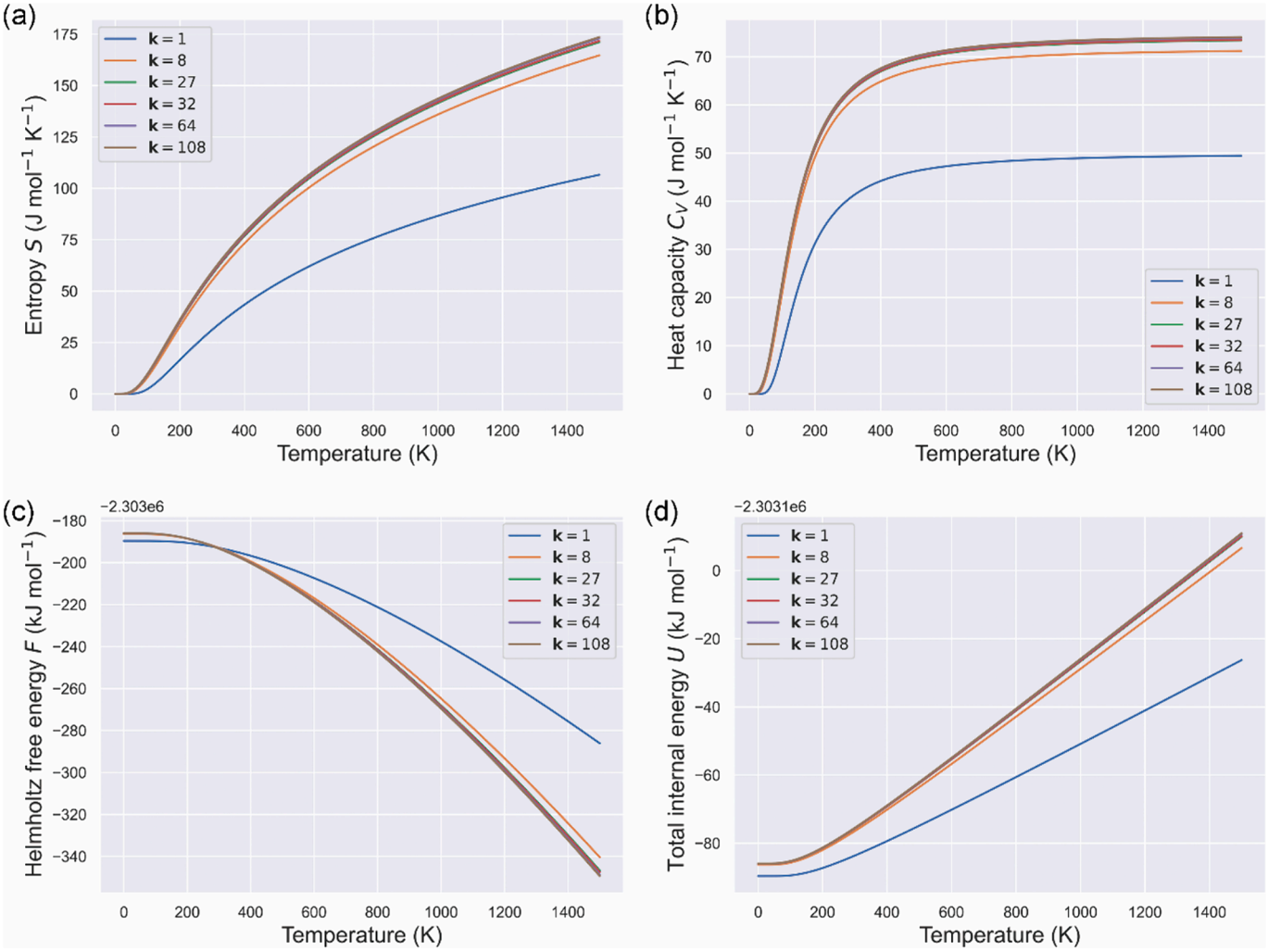

Fig. 5. Convergence of (a) entropy S, (b) isochoric heat capacity C_V, (c) Helmholtz free energy and (d) internal energy U of cubic CaF_2 as a function of the supercell size, i.e., number of **k** points used to sample the phonons of the mineral.

Table 3
Primitive cell volume V_{pc} (Å^3), bulk modulus K_T (GPa) and its first pressure derivative K' (dimensionless), coefficient of volumetric thermal expansion α_V ($\times 10^{-5}$ K^{-1}), entropy S (J mol^{-1} K^{-1}), isobaric C_P and isochoric C_V heat capacities (J mol^{-1} K^{-1}) and enthalpy $H-H^0_{298.15}$ (kJ/mol) as a function of temperature T (K) at 0 GPa. Differences with the experimental thermodynamic data of Chase [60] are reported as Δ (ΔS, ΔC_P, ΔH).

T (K)	V_{pc}	K_T	K'	α_V	S	ΔS	C_P	ΔC_P	C_V	$H-H^0_{298.15}$	ΔH
300	42.279	91.7	3.74	4.69	63.83	−5.23	65.43	−3.35	63.89	0.00	−0.14
400	42.485	90.1	3.68	5.05	83.42	−6.18	70.43	−3.19	68.08	6.83	−0.46
500	42.704	88.6	3.61	5.26	99.48	−6.82	73.30	−3.05	70.15	14.05	−0.75
600	42.932	87.2	3.54	5.38	113.04	−7.46	75.23	−3.46	71.31	21.50	−1.05
700	43.167	85.9	3.48	5.51	124.77	−8.03	76.77	−4.36	72.02	29.13	−1.41
800	43.407	84.6	3.41	5.60	135.12	−8.68	78.03	−5.81	72.48	36.89	−1.90
900	43.652	83.4	3.34	5.69	144.39	−9.41	79.19	−7.63	72.80	44.77	−2.55
1000	43.902	82.3	3.27	5.71	152.79	−10.31	80.12	−9.92	73.02	52.75	−3.41

$$P = K_{0T} f_E (1+2f_E)^{5/2}\left(1+\frac{3}{2}\left(K'_{0T}-4\right)fE+\frac{3}{2}\left(K_{0T}K''_{0T}+\left(K'_{0T}-4\right)\left(K'_{0T}-3\right)+\frac{35}{9}\right)f_E^2\right) \quad (10)$$

with K'' the second derivative of the bulk modulus with pressure and f_E the finite Eulerian strain, which is expressed as

$$f_E = \frac{1}{2}\left[\left(\frac{V_{0T}}{V_{PT}}\right)^{2/3}-1\right] \quad (11)$$

with V_{0T} the unit cell volume at zero pressure and temperature T and V_{PT} the unit cell volume at specific PT conditions. At the same time, the thermal expansion was treated using a modified Holland-Powell equation [62,63]

$$V_{0T} = V_{00}\left(1+\alpha_0\left(T-T_{ref}\right)-2(10\alpha_0+\alpha_1)\left(\sqrt{T}-\sqrt{T_{ref}}\right)\right) \quad (12)$$

with T_{ref} the reference temperature. Since the variation of the isothermal bulk modulus is almost linear in the 300 – 900 K range (see Fig. 7), the variation of the bulk modulus with temperature was considered constant, i.e., $\partial K_{0T}/\partial T$ = constant. The fitting procedure was

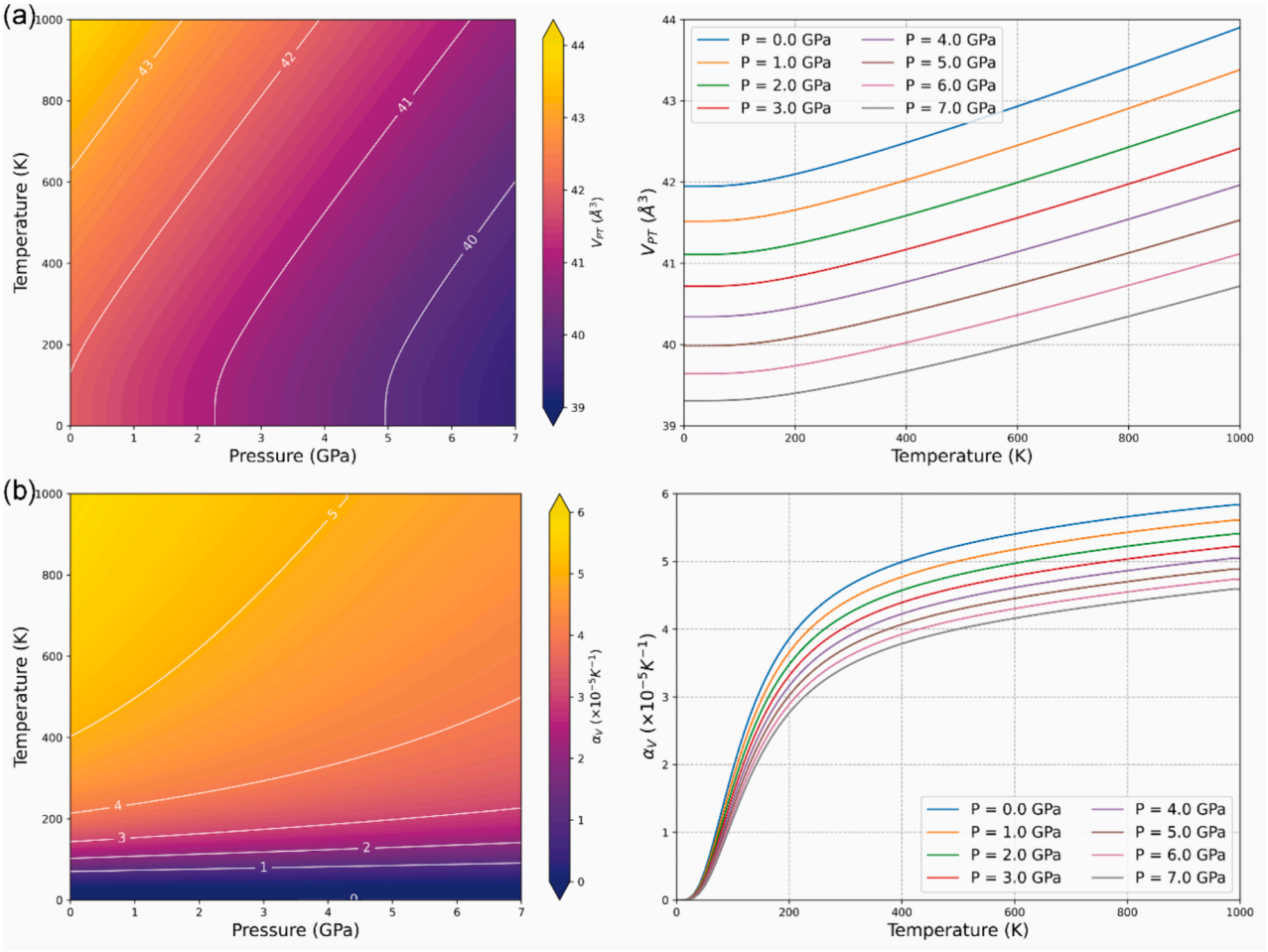

Fig. 6. Contour maps (on the left) and isobars (on the right) of fluorite related to the (a) unit cell volume V_{PT} and (b) coefficient of volumetric thermal expansion α_V between 0 GPa and 7 GPa and in the temperature range 0–1000 K.

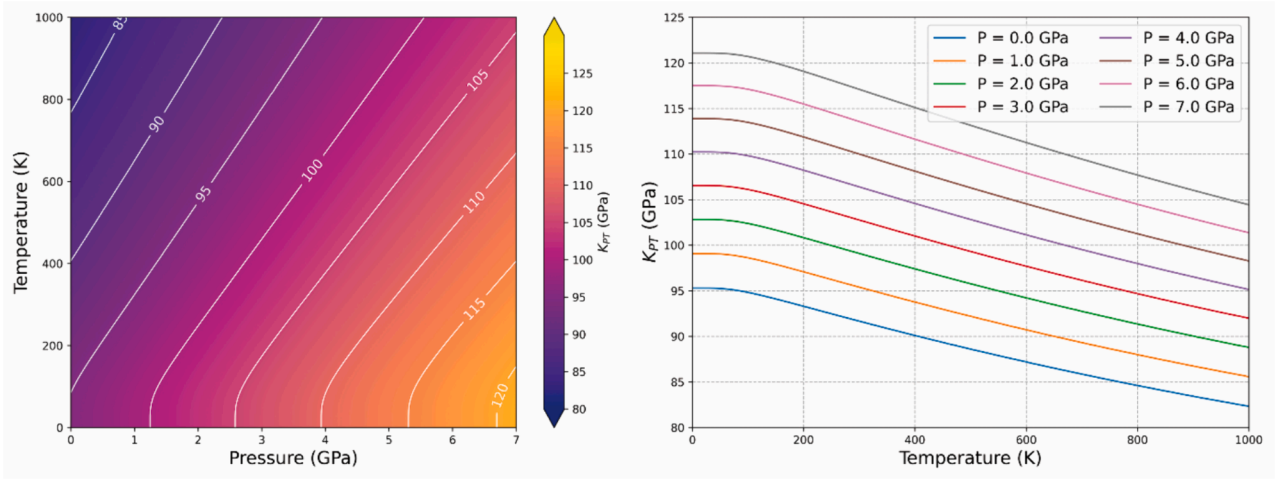

Fig. 7. Contour map (left panel) and isobars (right panel) of the isothermal bulk modulus K_{PT} of cubic CaF_2 calculated at the DFT/B3LYP level of theory in the *PT* ranges of 0–7 GPa and 0–1000 K, respectively.

performed setting $T_{ref} = 300$ K as the reference temperature, for which the calculated *PV* parameters were $V_{0T} = 42.278(7)$ Å^3, $K_{0T} = 92.14(7)$ GPa, $K'_{0T} = 3.56(2)$ and $K''_{0T} = -0.0395$. The K''_{0T} value is implied and it is not fitted in the third-order formulation of the Birch-Murnaghan equation of state. Regarding the thermal expansion, i.e., Eq. (12), the two parameters α_0 and α_1 obtained from the fitting procedure were 7.84 (2) × 10^{-5} K^{-1} and –2.17(3) × 10^{-5} K$^{-1/2}$. The parameter that links Eqs. (10) and (12) is the variation of the bulk modulus with temperature, whose constant value was calculated as $\partial K_{0T}/\partial T = -0.0160(1)$ GPa K^{-1}, a value in line with both the figure obtained from the polynomial fit (–0.0185 GPa K^{-1}, *vide supra*) and the previous estimations of $\partial K_{0T}/\partial T$, which were experimentally found between –0.0165 GPa K^{-1} and –0.031

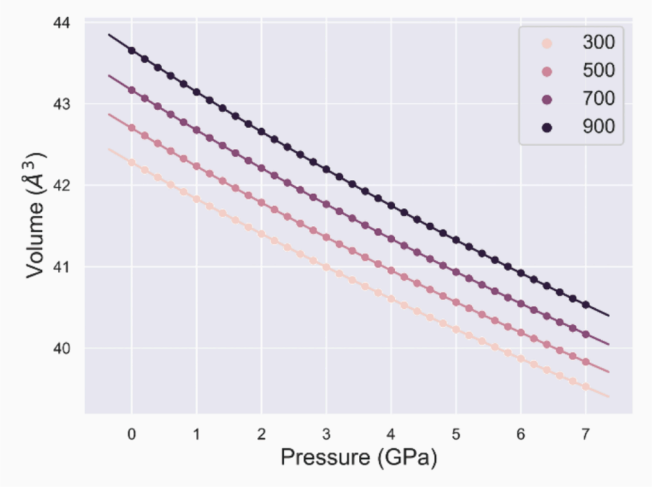

Fig. 8. Evolution of the unit cell volume of fluorite as a function of pressure, at different temperatures. The points are the values calculated at the DFT/B3LYP level of theory, whereas the lines curves obtained from the *PVT* equation of state fitting (see text for details).

GPa K^{-1} [6,57]. Using this knowledge, it is possible to derive the unit cell volume of fluorite as a function of pressure. In Fig. 8, it is reported the evolution of the unit cell volume of fluorite at different *PT* conditions using the *PVT* equation of state fitting results.

Finally, Fig. 9 reports the *PT* variations of entropy *S* and isobaric heat capacity C_P. Compared to the results of Chase [64], the theoretical DFT/B3LYP data are in satisfactory agreement, with an underestimation of about 5 % that could be related to the harmonic approximation used to calculate the phonon properties.

4. Conclusion

In the present work, a detailed characterization of the thermodynamic and thermoelastic features of cubic CaF_2, obtained within the quasi-harmonic approximation, was reported for the first time, extending the knowledge on this important mineral. Furthermore, fundamental information on the electronic properties of fluorite as a function of pressure was also presented, which can be useful for devising new applications for this phase in optics and electronics. The DFT/B3LYP results are generally in line with those obtained at the experimental level, with a slight overestimation of the bulk modulus K_{0T} and an underestimation of its first derivative with respect to pressure K'. This stiffer behaviour is a common figure experienced when using the LCAO approach for the calculation of the elastic properties, and is due to an overestimation of the forces acting on the model system because of the Pulay stress, which in turn arises from the incompleteness of the atomic

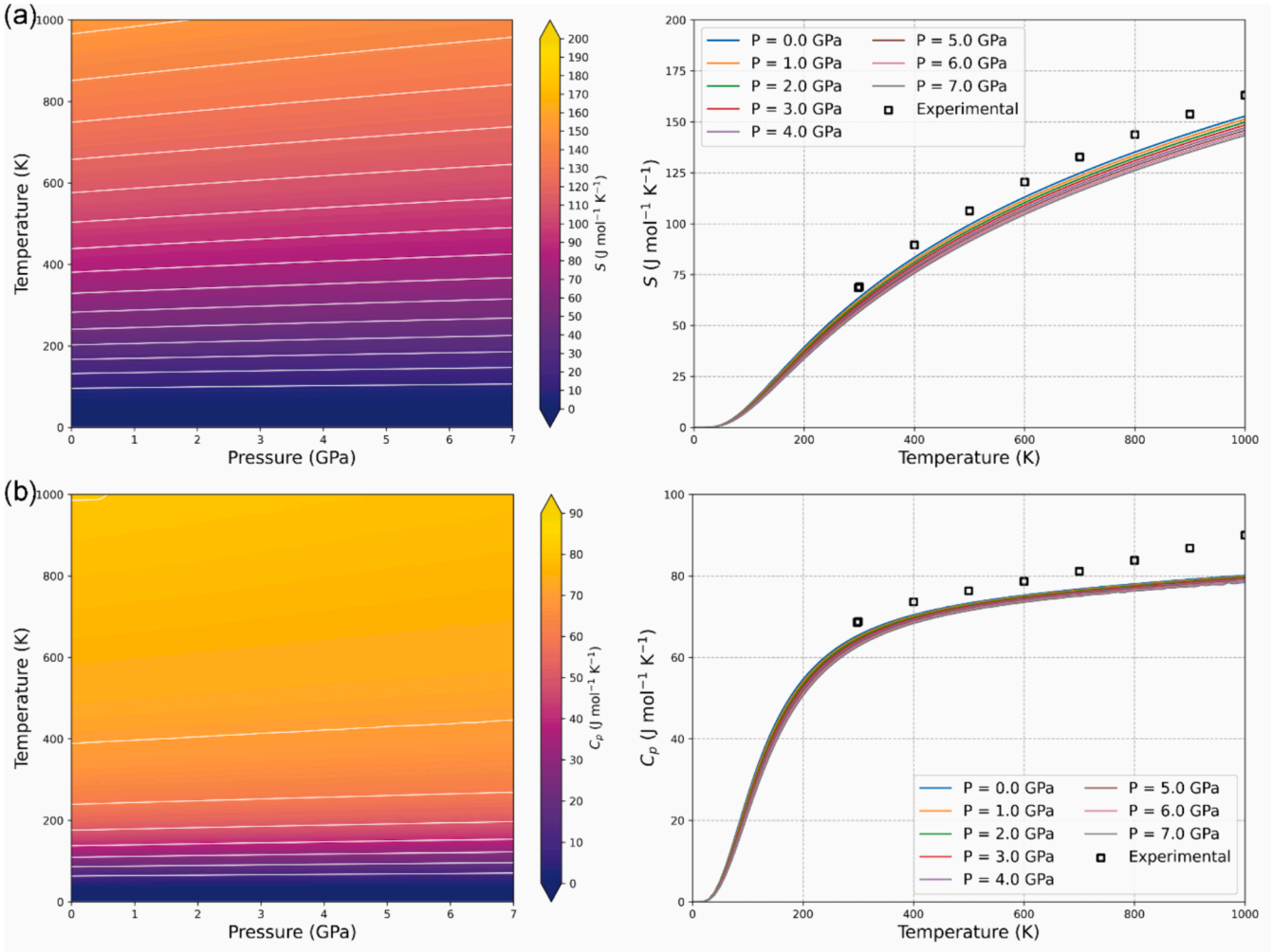

Fig. 9. Contour maps (on the left) and isobars (on the right) of (a) entropy S and (b) isobaric heat capacity C_P between 0 GPa and 7 GPa and in the temperature range 0–1000 K. The experimental results reported for a direct comparison are taken from the work of Chase [64].

basis set. Nevertheless, the employed approach is robust and provided an adequate description of the structural, electronic, vibrational features of fluorite, together with their derived quantities, i.e., thermodynamics and elastic properties in a wide pressure and temperature range. This kind of knowledge is useful in mineralogy, geology and, generally, in materials science, in particular when fluorite is employed as internal standard for high-pressure/high-temperature experiments.

Author contributions

Conceptualization, G.U. and G.V.; methodology, G.U.; validation, G. U. and G.V.; formal analysis, G.U.; investigation, G.U. and G.V.; data curation, G.U.; writing—review and editing, G.U. and G.V.; visualization, G.U.; supervision, G.V. All authors have read and agreed to the published version of the manuscript.

Funding sources

This research did not receive any specific grant from funding agencies in the public, commercial, or not-for-profit sectors.

CRediT authorship contribution statement

Gianfranco Ulian: Writing – review & editing, Writing – original draft, Visualization, Validation, Software, Methodology, Investigation, Formal analysis, Data curation, Conceptualization. **Giovanni Valdrè:** Writing – review & editing, Writing – original draft, Validation, Supervision, Resources, Methodology, Investigation, Formal analysis, Conceptualization.

Declaration of competing interest

The authors declare that they have no known competing financial interests or personal relationships that could have appeared to influence the work reported in this paper.

Data availability

Data will be made available on request.

Acknowledgment

The authors wish to thank the University of Bologna for supporting the present work.

References

[1] R.W.G. Wycoff Crystal structures. Vol. 1. 2nd ed. New York, London, Sydney: Interscience Publishers 1968.
[2] M. Letz, L. Parthier, Charge centers in CaF_2: ab initio calculation of elementary physical properties, Phys. Rev. B – Cond. Matter Mater. Phys. 74 (2006).
[3] J.H. Burnett, Z.H. Levine, E.L. Shirley, Intrinsic birefringence in calcium fluoride and barium fluoride, Phys. Rev. B – Cond. Matter Mater. Phys. 64 (2001).
[4] W. Huang, K. Nagayama, J. Yan, Fabrication of microlens arrays on single-crystal CaF2 by ultraprecision diamond turning, J. Mater. Process. Technol. 321 (2023).
[5] R.M. Hazen, L.W. Finger, High-temperature and high-pressure crystal chemistry, High-Pressure Res. Geosci. (1982) 151–176.
[6] R.J. Angel, The high-pressure, high-temperature equation of state of calcium fluoride, CaF_2, J. Phys. Condens. Matter 5 (1993) L141–L144.
[7] R.J. Angel, D.R. Allan, R. Milletich, L.W. Finger, The use of quartz as an internal pressure standard in high-pressure crystallography, J. Appl. Crystallogr. 30 (1997) 461–466.
[8] Miletich R, Allan DR, Kuhs WF. High-pressure single-crystal techniques. In: Hazen RM, Downs RT, editors. High-temperature and high-pressure crystal chemistry. Washington DC: Reviews in Mineralogy and Geochemistry, Mineralogical society of America; 2001. p. 445–519.
[9] L. Gerward, J.S. Olsen, L. Petit, G. Vaitheeswaran, V. Kanchana, A. Svane, Bulk modulus of CeO_2 and PrO_2 - an experimental and theoretical study, J. Alloy. Compd. 400 (2005) 56–61.
[10] J.P. Albert, C. Jouanin, C. Gout, Electronic band structure of fluorite, Phys. Rev. B 16 (1977) 925–933.
[11] M. Catti, A. Pavese, V.R. Saunders, Elastic constants and electronic structure of fluorite (CaF_2): an ab initio hartree-fock study, J. Phys. Condens. Matter. 3 (1991) 4151–4164.
[12] M. Mérawa, M. Llunell, R. Orlando, M. Gelize-Duvignau, R. Dovesi, Structural, electronic and elastic properties of some fluoride crystals: an ab initio study, Chem. Phys. Lett. 368 (2003) 7–11.
[13] D.M. Hoat, J.f rs, a mb., FP-LAPW investigation on structural, electronic and optical properties of Eu^{2+}-doped MF2 (M = Ca and Ba), Optik 161 (2018) 335–341.
[14] X.C. Yang, Y.W. Zhao, Z.M. Gao, X. Liu, L.X. Zhang, X.M. Wang, et al., First-principles study of structural stabilities, electronic and optical properties of CaF_2 under high pressure, Gaoya Wuli Xuebao/chinese J. High Pressure Phys. 24 (2010) 225–230.
[15] H. Shi, R. Jia, R.I. Eglitis, First-principles simulations of H centers in CaF_2, Comput. Mater. Sci 89 (2014) 247–256.
[16] Sharma SS. Thermal expansion of crystals: 11. magnetite and fluorite. Proceedings of the Indian Academy of Sciences, A31: 1950261–74.
[17] O.L. Anderson, Equation of state of solids for geophysics and ceramic science, Oxford University Press, New York, US, 1995.
[18] R. Dovesi, A. Erba, R. Orlando, C.M. Zicovich-Wilson, B. Civalleri, L. Maschio, et al., Quantum-mechanical condensed matter simulations with CRYSTAL, Wiley Interdis. Reviews-Computational Mol. Sci. 8 (2018) E1360.
[19] A.D. Becke, Density-functional thermochemistry. 3. the role of exact exchange, J. Chem. Phys. 98 (1993) 5648–5652.
[20] A.D. Becke, A New mixing of hartree-fock and local density-functional theories, J. Chem. Phys. 98 (1993) 1372–1377.
[21] C.T. Lee, W.T. Yang, R.G. Parr, Development of the colle-salvetti correlation-energy formula into a functional of the electron-density, Phys. Rev. B 37 (1988) 785–789.
[22] D. Belmonte, First principles thermodynamics of minerals at HP-HT conditions: MgO as a prototypical material, Minerals 7 (2017) 183.
[23] B. Civalleri, K. Doll, C.M. Zicovich-Wilson, Ab initio investigation of structure and cohesive energy of crystalline urea, J. Phys. Chem. B 111 (2007) 26–33.
[24] A. Erba, A. Mahmoud, D. Belmonte, R. Dovesi, High pressure elastic properties of minerals from ab initio simulations: the case of pyrope, grossular and andradite silicate garnets, J. Chem. Phys. 140 (2014) 124703.
[25] F. Pascale, C.M. Zicovich-Wilson, R. Orlando, C. Roetti, P. Ugliengo, R. Dovesi, Vibration frequencies of $Mg_3Al_2Si_3O_{12}$ pyrope. an ab initio study with the CRYSTAL code, J. Phys. Chem. B 109 (2005) 6146–6152.
[26] M. Prencipe, I. Scanavino, F. Nestola, M. Merlini, B. Civalleri, M. Bruno, et al., High-pressure thermo-elastic properties of beryl ($Al_4Be_6Si_{12}O_{36}$) from ab initio calculations, and observations about the source of thermal expansion, Phys. Chem. Miner. 38 (2011) 223–239.
[27] G. Ulian, G. Valdrè, Thermomechanical, electronic and thermodynamic properties of ZnS cubic polymorphs: an *ab initio* investigation on the zinc-blende – rock-salt phase transition, Acta Crystallogr. B 75 (2019) 1042–1059.
[28] G. Ulian, G. Valdrè, The effect of long-range interactions on the infrared and Raman spectra of aragonite ($CaCO_3$, *Pmcn*) up to 25 GPa, Sci. Rep. 13 (2023) 2725.
[29] D. Vilela Oliveira, J. Laun, M.F. Peintinger, T. Bredow, BSSE-correction scheme for consistent gaussian basis sets of double- and triple-zeta valence with polarization quality for solid-state calculations, J. Comput. Chem. 40 (2019) 2364–2376.
[30] M.D. Towler, A. Zupan, M. Causà, Density functional theory in periodic systems using local gaussian basis sets, Comput. Phys. Commun. 98 (1996) 181–205.
[31] H.J. Monkhorst, J.D. Pack, Special points for brillouin-zone integrations, Phys. Rev. B 8 (1976) 5188–5192.
[32] F. Pascale, C.M. Zicovich-Wilson, F.L. Gejo, B. Civalleri, R. Orlando, R. Dovesi, The calculation of the vibrational frequencies of crystalline compounds and its implementation in the CRYSTAL code, J. Comput. Chem. 25 (2004) 888–897.
[33] S. Tosoni, F. Pascale, P. Ugliengo, R. Orlando, V.R. Saunders, R. Dovesi, Quantum mechanical calculation of the OH vibrational frequency in crystalline solids, Mol. Phys. 103 (2005) 2549–2558.
[34] A. Erba, On combining temperature and pressure effects on structural properties of crystals with standard ab initio techniques, J. Chem. Phys. 141 (2014) 124115.
[35] G. Ulian, D. Moro, G. Valdrè, Thermodynamic and thermoelastic properties of wurtzite-ZnS by density functional theory, Am. Mineral. 105 (2020) 1212–1222.
[36] M.T. Dove, Introduction to Lattice Dynamics, Cambridge University Press, 1993.
[37] K. Parlinski, Z.Q. Li, Y. Kawazoe, First-principles determination of the soft mode in cubic ZrO_2, Phys. Rev. Lett. 78 (1997) 4063–4066.
[38] D.W. Wallace, Thermodynamics of Crystals, Dover Publications, 1998.
[39] Y. Wang, J.J. Wang, W.Y. Wang, Z.G. Mei, S.L. Shang, L.Q. Chen, et al., A mixed-space approach to first-principles calculations of phonon frequencies for polar materials, J. Physics-Condensed Matter 22 (2010).
[40] L. Maschio, B. Kirtman, R. Orlando, M. Rerat, Ab initio analytical infrared intensities for periodic systems through a coupled perturbed Hartree-Fock/Kohn-Sham method, J. Chem. Phys. 137 (2012) 204113.
[41] R. Orlando, V. Lacivita, R. Bast, K. Ruud, Calculation of the first static hyperpolarizability tensor of three-dimensional periodic compounds with a local basis set: a comparison of LDA, PBE, PBE0, B3LYP, and HF results, J. Chem. Phys. 132 (2010) 244106.
[42] G. Ottonello, B. Civalleri, J. Ganguly, M.V. Zuccolini, Y. Noel, Thermophysical properties of the α–β–γ polymorphs of Mg_2SiO_4: a computational study, Phys. Chem. Miner. 36 (2009) 87–106.
[43] G. Ulian, G. Valdre, Equation of state of hexagonal hydroxylapatite (P6(3)) as obtained from density functional theory simulations, Int. J. Quantum. Chem. 118 (2018) e25553.
[44] G. Ulian, G. Valdrè, QUANTAS, a Python software for the analysis of solids from ab initio quantum mechanical simulations and experimental data, J. Appl. Crystallogr. 55 (2022) 386–396.

[45] F. Birch, Finite elastic strain of cubic crystal, Phys. Rev. 71 (1947) 809–824.
[46] M. Hebbache, M. Zemzemi, Ab initio study of high-pressure behavior of a low compressibility metal and a hard material: osmium and diamond, Phys. Rev. B 70 (2004).
[47] R. Khenata, B. Daoudi, M. Sahnoun, H. Baltache, M. Rérat, A.H. Reshak, et al., Structural, electronic and optical properties of fluorite-type compounds, Eur. Phys. J. B 47 (2005) 63–70.
[48] V. Kanchana, G. Vaitheeswaran, M. Rajagopalan, Structural phase stability of CaF_2 and SrF_2 under pressure, Phys. B Condens. Matter 328 (2003) 283–290.
[49] A.M. Pendás, J.M. Recio, M. Flórez, V. Luaña, M. Bermejo, Static simulations of CaF_2 polymorphs, Phys. Rev. B 49 (1994) 5858–5868.
[50] W.Y. Ching, F. Gan, M.-Z. Huang, Band theory of linear and nonlinear susceptibilities of some binary ionic insulators, Phys. Rev. B 52 (1995) 1596–1611.
[51] R.T. Poole, J. Szajman, R.C.G. Leckey, J.G. Jenkin, J. Liesegang, Electronic structure of the alkaline-earth fluorides studied by photoelectron spectroscopy, Phys. Rev. B 12 (1975) 5872–5877.
[52] W.A. Harrison, Electronic structure and the properties of solids: the physics of the chemical bond, Dover Publications, San Francisco, CA, 1980.
[53] P. Denham, G.R. Field, P.L.R. Morse, G.R. Wilkinson, Optical and dielectric properties and lattice dynamics of some fluorite structure ionic crystals, Proc. R. Soc. Lond. A 317 (1970) 55–77.
[54] J.R. Kassier, E. Monberg, M. Nicol, Studies of fluorite and related divalent fluoride systems at high pressure by raman spectroscopy, J. Chem. Phys. (1974) 5057–5065.
[55] R.P. Lowndes, Anharmonicity in the alkaline earth fluorides, J. Phys. C Solid State Phys. 4 (1971) 3083–3094.
[56] S. Speziale, T.S. Duffy, Single-crystal elastic constants of fluorite (CaF_2) to 9.3 GPa, Phys. Chem. Miner. 29 (2002) 465–472.
[57] K. Schmalzl, D. Strauch, H. Schober, Lattice-dynamical and ground-state properties of CaF_2 studied by inelastic neutron scattering and density-functional methods, Phys. Rev. B – Condens. Matter Mater. Phys. 68 (2003).
[58] Y. Wang, L.A. Zhang, S. Shang, Z.K. Liu, L.Q. Chen, Accurate calculations of phonon dispersion in CaF_2 and CeO_2, Phys. Rev. B – Condens. Matter Mater. Phys. 88 (2013).
[59] B. Schumann, H. Neumann, Thermal expansion of CaF_2 from 298 to 1173 K, Cryst. Res. Technol. 19 (1984) K13–K14.
[60] G. Ulian, G. Valdrè, Second-order elastic constants of hexagonal hydroxylapatite ($P6_3$) from ab initio quantum mechanics: comparison between DFT functionals and basis sets, Int. J. Quantum. Chem. 118 (2018) e25500.
[61] R.J. Angel, J. Gonzalez-Platas, M. Alvaro, EosFit7c and a Fortran module (library) for equation of state calculations, Z. Kristallogr. 229 (2014) 405–419.
[62] T.J.B. Holland, R. Powell, An internally consistent thermodynamic data set for phases of petrological interest, J. Metam. Geol. 16 (1998) 309–343.
[63] A.R. Pawley, S.A.T. Redfern, T.J.B. Holland, Volume behavior of hydrous minerals at high pressure and temperature.1. thermal expansion of lawsonite, zoisite, clinozoisite, and diaspore, Am. Mineral. 81 (1996) 335–340.
[64] M.W.Jr. Chase, NIST-JANAF Thermochemical Tables Fourth ed, Journal of Physical and Chemical Reference Data, Monograph 9 (1998).